

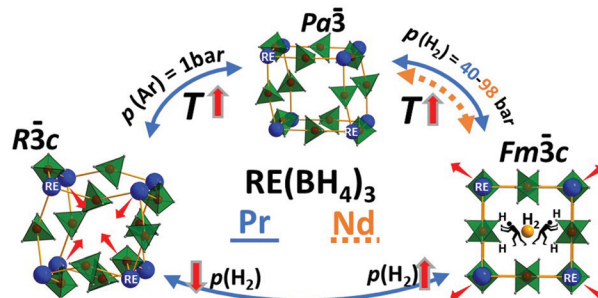
We have presented the Graphical Abstract text and image for your article below. This brief summary of your work will appear in the contents pages of the issue in which your article appears.

1

Synthesis, structure, and polymorphic transitions of praseodymium(III) and neodymium(III) borohydride, $\text{Pr}(\text{BH}_4)_3$ and $\text{Nd}(\text{BH}_4)_3$

SeyedHosein Payandeh GharibDoust,* Michael Heere, Carlo Nervi, Magnus H. Sørby, Bjørn C. Hauback and Torben R. Jensen*

In this work, praseodymium(III) borohydride, $\text{Pr}(\text{BH}_4)_3$, and an isotopically enriched analogue, $\text{Pr}^{(11}\text{BD}_4)_3$, are prepared by a new route *via* a solvate complex, $\text{Pr}^{(11}\text{BD}_4)_3\text{S}(\text{CH}_3)_2$.



Please check this proof carefully. **Our staff will not read it in detail after you have returned it.**

Proof corrections must be returned as a single set of corrections, approved by all co-authors. No further corrections can be made after you have submitted your proof corrections as we will publish your article online as soon as possible after they are received.

Please ensure that:

- The spelling and format of all author names and affiliations are checked carefully. Names will be indexed and cited as shown on the proof, so these must be correct.
- Any funding bodies have been acknowledged appropriately.
- All of the editor's queries are answered.
- Any necessary attachments, such as updated images or ESI files, are provided.

Translation errors between word-processor files and typesetting systems can occur so the whole proof needs to be read. Please pay particular attention to: tables; equations; numerical data; figures and graphics; and references.

Please send your corrections preferably as a copy of the proof PDF with electronic notes attached or alternatively as a list of corrections – do not change the text within the PDF file or send a revised manuscript. Corrections at this stage should be minor and not involve extensive changes.

Please return your **final** corrections, where possible within **48 hours** of receipt, by e-mail to: dalton@rsc.org. If you require more time, please notify us by email.

Funder information

Providing accurate funding information will enable us to help you comply with your funders' reporting mandates. Clear acknowledgement of funder support is an important consideration in funding evaluation and can increase your chances of securing funding in the future. We work closely with Crossref to make your research discoverable through the Funding Data search tool (<http://search.crossref.org/funding>).

Further information on how to acknowledge your funders can be found on our webpage (<http://rsc.li/funding-info>).

What is Funding Data?

Funding Data (<http://www.crossref.org/fundingdata/>) provides a reliable way to track the impact of the work that funders support. We collect funding information from our authors and match this information to funders listed in the Crossref Funder Registry. Once an article has been matched to its funders, it is discoverable through Crossref's search interface.

PubMed Central

Accurate funder information will also help us identify articles that are mandated to be deposited in PubMed Central (PMC) and deposit these on your behalf.

Providing funder information

We have combined the information you gave us on submission with the information in your acknowledgements. This will help ensure funding information is as complete as possible and matches funders listed in the Crossref Funder Registry. **Please check that the funder names and grant numbers in the table are correct.** This table will not be included in your final PDF but we will share the data with Crossref so that your article can be found *via* the Funding Data search tool.

Funder name	Funder ID (for RSC use only)	Award/grant/contract number
FP7 People: Marie-Curie Actions	100011264	607040
Danmarks Grundforskningsfond	501100001732	Unassigned
Det Frie Forskningsråd	501100004836	DFF – 4181-00462
Carlsbergfondet	501100002808	Unassigned

Q1

If a funding organisation you included in your acknowledgements or on submission of your article is not currently listed in the registry it will not appear in the table above. We can only deposit data if funders are already listed in the Crossref Funder Registry, but we will pass all funding information on to Crossref so that additional funders can be included in future.

Researcher information

If any authors have ORCID or ResearcherID details that are not listed below, please provide these with your proof corrections. Please check that the ORCID and ResearcherID details listed below have been assigned to the correct author. Authors should have their own unique ORCID iD and should not use another researcher's, as errors will delay publication.

Please also update your account on our online manuscript submission system to add your ORCID details, which will then be automatically included in all future submissions. See [here](#) for step-by-step instructions and more information on author identifiers.

First (given) name(s)	Last (family) name(s)	ResearcherID	ORCID
SeyedHosein	Payandeh GharibDoust		0000-0003-2828-7106
Michael	Heere		0000-0002-7826-1425
Carlo	Nervi	B-1355-2008	0000-0002-3712-7369
Magnus H.	Sørby		0000-0002-8878-3331
Bjørn C.	Hauback		
Torben R.	Jensen		0000-0002-4278-3221

Queries for the attention of the authors

Journal: **Dalton Transactions** Paper: **c8dt00118a**

Title: **Synthesis, structure, and polymorphic transitions of praseodymium(III) and neodymium(III) borohydride, Pr(BH₄)₃ and Nd(BH₄)₃**

For your information: You can cite this article before you receive notification of the page numbers by using the following format: (authors), Dalton Trans., (year), DOI: 10.1039/c8dt00118a.

Editor's queries are marked like this [Q1, Q2, ...], and for your convenience line numbers are indicated like this [5, 10, 15, ...].


Please ensure that all queries are answered when returning your proof corrections so that publication of your article is not delayed.

Query Reference	Query	Remarks
Q1	Funder details have been incorporated in the funder table using information provided in the article text. Please check that the funder information in the table is correct.	The numbers are correct
Q2	Please confirm that the spelling and format of all author names is correct. Names will be indexed and cited as shown on the proof, so these must be correct. No late corrections can be made.	The author names are correct.
Q3	Please check that the inserted Graphical Abstract text is suitable. Please ensure that the text fits between the two horizontal lines.	The inserted graphical abstract is suitable
Q4	The citation to Table 2 in the sentence beginning "A new solvate..." has been changed to Table 1 as the text appears to discuss Table 1. Please check that this is correct.	No Please change the text to Table 2.
Q5	Please check that the footnotes a has been displayed correctly in Table 2.	Please write a after (A) "RE-B (A) a"
Q6	Please note that a conflict of interest statement is required for all manuscripts. Please read our policy on Conflicts of interest (http://rsc.li/conflicts) and provide a statement with your proof corrections. If no conflicts exist, please state that "There are no conflicts to declare".	There are no conflicts to declare.

PAPER

Synthesis, structure, and polymorphic transitions
of praseodymium(III) and neodymium(III)
borohydride, $\text{Pr}(\text{BH}_4)_3$ and $\text{Nd}(\text{BH}_4)_3$ †

Cite this: DOI: 10.1039/c8dt00118a

SeyedHosein Payandeh GharibDoust,^{*a} Michael Heere,^{b,c} Carlo Nervi,^d
Magnus H. Sørby,^b Bjørn C. Hauback^b and Torben R. Jensen^b  ^{*a}

In this work, praseodymium(III) borohydride, $\text{Pr}(\text{BH}_4)_3$, and an isotopically enriched analogue, $\text{Pr}^{11}\text{BD}_4)_3$, are prepared by a new route via a solvate complex, $\text{Pr}^{11}\text{BD}_4)_3\text{S}(\text{CH}_3)_2$. $\text{Nd}(\text{BH}_4)_3$ was synthesized using the same method and the structures, polymorphic transformations, and thermal stabilities of these compounds are investigated in detail. $\alpha\text{-Pr}(\text{BH}_4)_3$ and $\alpha\text{-Nd}(\text{BH}_4)_3$ are isostructural with cubic unit cells ($P\bar{a}3$) stable at room temperature (RT) and a unit cell volume per formula unit (V/Z) of 180.1 and 175.8 Å³, respectively. Heating $\alpha\text{-Pr}(\text{BH}_4)_3$ to $T \sim 190$ °C, $p(\text{Ar}) = 1$ bar, introduces a transition to a rhombohedral polymorph, $r\text{-Pr}(\text{BH}_4)_3$ ($R\bar{3}c$) with a smaller unit cell volume and a denser structure, $V/Z = 156.06$ Å³. A similar transition was not observed for $\text{Nd}(\text{BH}_4)_3$. However, heat treatment of $\alpha\text{-Pr}(\text{BH}_4)_3$, at $T \sim 190$ °C, $p(\text{H}_2) = 40$ bar and $\alpha\text{-Nd}(\text{BH}_4)_3$, at $T \sim 270$ °C, $p(\text{H}_2) = 98$ bar facilitates reversible formation of another three cubic polymorph, denoted as β , β' and $\beta''\text{-RE}(\text{BH}_4)_3$ ($Fm\bar{3}c$). Moreover, the transition β - to β' - to β'' - is considered a rare example of stepwise negative thermal expansion. For $\text{Pr}(\text{BH}_4)_3$, $\sim 2/3$ of the sample takes this route of transformation whereas in argon only ~ 5 wt%, and the remaining transforms directly from α - to $r\text{-Pr}(\text{BH}_4)_3$. The β -polymorphs are porous with $V/Z = 172.4$ and 172.7 Å³ for $\beta''\text{-RE}(\text{BH}_4)_3$, RE = Pr or Nd, respectively, and are stabilized by the elevated hydrogen pressures. The polymorphic transitions occur due to rotation of $\text{RE}(\text{BH}_4)_6$ octahedra without breaking or forming chemical bonds. Structural DFT optimization reveals the decreasing stability of $\alpha\text{-Pr}(\text{BH}_4)_3 > \beta\text{-Pr}(\text{BH}_4)_3 > r\text{-Pr}(\text{BH}_4)_3$.

Received 10th January 2018,

Accepted 14th May 2018

DOI: 10.1039/c8dt00118a

rsc.li/dalton

1. Introduction

One of the greatest challenges in the 21st century is the transition towards a sustainable and environmentally friendly energy system.^{1,2} Hydrogen is the most abundant and lightest element and has the highest gravimetric energy density for any known substance. Hydrogen is therefore an ideal (renewable) energy carrier.^{3–5} Metal borohydrides have received considerable attention as potential hydrogen storage materials due to their high hydrogen densities.^{6,7} A wide variety of metal borohydrides have been synthesized and characterized,

and an inverse correlation has been found between the decomposition temperature of the metal borohydride and the Pauling electronegativity of the metal.^{7,8} In recent years, rare-earth (RE) metal borohydrides, in particular, have received considerable interest due to their various properties.^{9–14} RE $(\text{BH}_4)_2(\text{THF})_2$ (RE = Eu and Yb, THF = tetrahydrofuran) have shown high luminescence properties,¹⁵ and other lanthanide borohydride complexes such as $\text{RE}(\text{BH}_4)_3(\text{THF})_3$ (RE = Nd, Sm) have been used extensively for the catalysis of organic polymerization reactions.^{16–18} These compounds have a higher solubility in apolar solvents compared to that of traditional $\text{RECl}_3(\text{THF})_3$ compounds, which makes them promising candidates as catalysts.^{16–18} The hydrogen capacities of rare-earth metal borohydrides, $\text{RE}(\text{BH}_4)_n$, $n = 2, 3$, vary between 9.07 wt% H₂ for $\text{Yb}(\text{BH}_4)_3$ to 5.56 wt% for $\text{Yb}(\text{BH}_4)_3$,^{19–24} and are within the range of MgH_2 (7.65 wt% H₂) and NaAlH_4 (7.46 wt% H₂), which have previously received considerable attention.^{25,26} Bimetallic rare-earth borohydrides such as $\text{MY}(\text{BH}_4)_4$, M = Li, Na, and $\text{LiRE}(\text{BH}_4)_3\text{Cl}$, RE = La, Ce, Gd have moderate to high Li and Na ion conductivity.^{12,13,27–31} Magnetocaloric properties have also been observed for $\text{K}_2\text{Gd}(\text{BH}_4)_5$ and $\text{Cs}_3\text{Gd}(\text{BH}_4)_6$.³²

^aCenter for Materials Crystallography, Interdisciplinary Nanoscience Center (iNANO) and Department of Chemistry, Aarhus University, Langelandsgade 140,

DK-8000 Århus C, Denmark. E-mail: a.payande88@gmail.com, trj@chem.au.dk

^bPhysics Department, Institute for Energy Technology, NO-2027 Kjeller, Norway

^cResearch Neutron Source Munich (FRM2) and Karlsruhe Institute of Technology (KIT), Institute for Applied Materials—Energy Storage Systems (IAM-ESS), 76344 Eggenstein, Germany

^dDepartment of Chemistry, NIS and CIRCC, University of Turin, Via P. Giuria 9, I-10125 Torino, Italy

† Electronic supplementary information (ESI) available. See DOI: 10.1039/c8dt00118a

The crystal chemistry of rare-earth metal borohydrides, $\text{RE}(\text{BH}_4)_3$, is diverse and interesting.^{5,33} Metal borohydrides with the largest cations, RE = La, Ce, crystallize in the trigonal crystal system with space group $R\bar{3}c$ ($r\text{-RE}(\text{BH}_4)_3$).^{13,34} Smaller cations, e.g. Pr to Yb, crystallize in the cubic crystal system with space group $Pa\bar{3}$ ($\alpha\text{-RE}(\text{BH}_4)_3$).^{19,23,35} Most of the trivalent rare-earth borohydrides undergo a transition to a second cubic polymorph with space group symmetry either $Pm\bar{3}m$ or $Fm\bar{3}c$ at elevated temperatures ($\beta\text{-RE}(\text{BH}_4)_3$).^{19,23,35–39} All known RE $(\text{BH}_4)_3$ with space group symmetry $Pa\bar{3}$, $R\bar{3}c$, $Pm\bar{3}m$, or $Fm\bar{3}c$ have crystal structures related to polymorphs of rhenium trioxide, ReO_3 .^{33,34} Some rare-earth metals form stable borohydrides in oxidation state(II), e.g. Sm^{2+} and Eu^{2+} , which crystallize in the orthorhombic crystal system (space group $Pbcn$) at RT. Upon heating, europium(II) borohydride, $\text{Eu}(\text{BH}_4)_2$, transforms into tetragonal and cubic polymorphs with space group symmetry $P4_12_12$ and $Fm\bar{3}m$, respectively.^{21,24}

Previous methods for the synthesis of trivalent rare-earth metal borohydrides were based on the reaction of LiBH_4 with RECl_3 ,^{23,34} but the products obtained using this method were contaminated with amorphous LiBH_4 . The presence of amorphous LiBH_4 has consequences for thermal properties and chemical reactivity of samples prepared by this method. For example, $\text{La}(\text{BH}_4)_3$ synthesized according to this method formed $\text{Li}_3\text{K}_3\text{La}_2(\text{BH}_4)_{12}$ upon reaction with KBH_4 .¹³ Therefore, our focus has been on new synthetic strategies and investigation of chemical, physical, and structural properties of the pure compounds. Here we present a new method to obtain solvate complexes, $\text{RE}(\text{BH}_4)_3\text{S}(\text{CH}_3)_2$, RE = Pr, Nd, and the corresponding borohydrides, $\text{Pr}(\text{BH}_4)_3$, $\text{Nd}(\text{BH}_4)_3$, which allows detailed investigation of the polymorphic transformations.

2. Experimental

2.1 Sample preparation

$\text{Pr}(\text{BH}_4)_3$ and $\text{Nd}(\text{BH}_4)_3$ compounds were synthesized using a new method based on the reaction of PrH_3 or NdH_3 with a dimethyl sulfide borane complex, $\text{S}(\text{CH}_3)_2\text{BH}_3$ (DMS). RE metal ingots were scrapped with sand paper to remove the oxide layer, placed in an autoclave, and heated up to 380 °C for 2 hours under hydrogen pressure $p(\text{H}_2) = 100$ bar to form REH_3 (RE = Pr, Nd). The formation of REH_3 was confirmed by X-ray powder diffraction (XRPD). However, the hydrogenation was repeated for the second time in order to prevent contamination of the sample with the RE metal. In the next step, the REH_3 (RE = Pr, Nd) powder was ball milled for two hours under an argon atmosphere (10 min milling, 2 min break, 12 repetitions) with a powder-to-ball ratio of 1:20. A Fritsch Pulverisette 6 planetary ball mill was used, which was equipped with a tungsten carbide vial (80 mL) and balls (o.d. 10 mm).

The ball-milled powder was transferred to a reaction flask and mixed with $\text{S}(\text{CH}_3)_2\text{BH}_3$ in a toluene solvent (10 M) at a molar ratio of 1:4.5. The excess of the $\text{S}(\text{CH}_3)_2\text{BH}_3$ solvent was used to completely consume the REH_3 , and the solution was

diluted to half-concentration by adding the same volume of toluene. The mixture was stirred for 2 days at 45 °C. Then the temperature was decreased to 35 °C and dimethyl sulfide was added to the mixture (50 mL per gram of REH_3) in order to dissolve $\text{RE}(\text{BH}_4)_3\text{S}(\text{CH}_3)_2$, allowing the removal of possible remaining REH_3 in the sample. After one day of stirring at 35 °C, the solution was filtered, and the solvent was removed using a rotary evaporator at 70 °C.

At this stage, $\text{RE}(\text{BH}_4)_3\text{S}(\text{CH}_3)_2$ (RE = Pr, Nd) was obtained. In order to remove the coordinated solvent, the powder was transferred to a glass tube and annealed at 180 °C under vacuum for 1 h. The sample was then ground with a mortar and pestle in a glovebox. The heat treatment was repeated once more in order to completely remove the DMS solvent from the sample.

An isotopically enriched sample of praseodymium(III) borohydride, $\text{Pr}^{(11}\text{BD}_4)_3$, was prepared using the same procedure with different reagents. For deuteration, the Pr ingots were transferred to an autoclave placed in liquid nitrogen and deuterium, D_2 , gas was added ($p(\text{D}_2) = 8$ bar) and the pressure increased to $p(\text{D}_2) = 14$ bar upon heating the autoclave from room temperature (RT). The autoclave was then heated further to 390 °C for 2 hours. The deuteration procedure was repeated three times in order to fully convert the Pr metal to PrD_3 . The solvated praseodymium(III) borohydride was prepared using $\text{S}(\text{CH}_3)_2^{(11}\text{BD}_3)$ and using the same procedures as described above.

LiBH_4 (95%), toluene, $\text{C}_6\text{H}_5\text{CH}_3$ (anhydrous, 99.8%), dimethyl sulfide, DMS, $\text{S}(\text{CH}_3)_2$ (anhydrous, 99.9%), and praseodymium, Pr (99.9%), and Neodymium, Nd (99.9%), ingots were purchased from Sigma-Aldrich. $\text{S}(\text{CH}_3)_2\text{BH}_3$ and $\text{S}(\text{CH}_3)_2^{(11}\text{BD}_3)$ (10.0 M in toluene) were purchased from Katchem. All chemicals were used as received and sample manipulation was performed in an argon-filled glove box with a circulation purifier, (O_2 , H_2O) < 0.5 ppm.

2.2 In situ synchrotron radiation X-ray powder diffraction

In situ synchrotron radiation X-ray powder diffraction (SR-XRPD) data of the samples were collected at the Swiss-Norwegian Beam Line (SNBL, BM01A) at ESRF, Grenoble, France, and at the P02 beamline at Petra III, Desy, Hamburg, Germany. At SNBL, a Dexela-PerkinElmer 2923 CMOS pixel detector⁴⁰ was used, and the wavelength was 0.7129 Å. At Petra III, a PerkinElmer XRD1621 detector was used, and the selected X-ray wavelength was 0.2072 Å. The samples were mounted in boron silicate capillaries (o.d. 0.5 mm) under argon and sealed with glue to prevent contact with air. For the *in situ* XRPD experiment under pressure which was performed in ESRF, the sample was loaded in a quartz capillary (o.d. 0.5 mm) and attached to a specially designed sample holder from ESRF, and hydrogen gas was applied, $p(\text{H}_2) = 40$ bar. For the high-pressure experiments performed in the P02 beamline at Petra III, samples were packed in sapphire tubes (i.d. 0.8 mm) and attached to a specially designed sample cell for studying solid-gas reactions, and hydrogen gas was applied, $p(\text{H}_2) = 98$ bar.^{41,42}

2.3 Neutron powder diffraction

Neutron powder diffraction (NPD) data of the $\text{Pr}^{(11}\text{BD}_4)_3$ sample were collected at two different places, the spallation neutron source SINQ at the Paul Scherrer Institute in Villigen, Switzerland and the JEEP II reactor at the Institute for Energy Technology in Kjeller, Norway. At SINQ, NPD data were collected at a high-resolution powder neutron diffractometer (HRPT) from $2\theta = 10^\circ$ to 130° .⁴³ The powder sample was enclosed in a vanadium can (8 mm diameter), and data were collected with a wavelength of $\lambda = 1.494 \text{ \AA}$. At the JEEP II reactor, data were collected using a PUS instrument and neutrons with $\lambda = 1.5583 \text{ \AA}$ were obtained from a Ge (511) focusing monochromator. Data were collected from 10° to 130° in steps of 0.05° in 2θ .⁴⁴

2.4 Structure solution and refinement

A new solvate compound and new polymorphs of $\text{Pr}(\text{BH}_4)_3$, rhombohedral $r\text{-Pr}(\text{BH}_4)_3$ ($R\bar{3}c$) and cubic $\beta\text{-Pr}(\text{BH}_4)_3$ ($Fm\bar{3}c$), were identified and structurally characterized in this investigation, see Table 1 and Tables S2, S3.† Moreover, a new high-temperature polymorph of $\text{Nd}(\text{BH}_4)_3$ ($Fm\bar{3}c$) was identified. Structural models for the new compounds were derived from isostructurally known compounds as discussed in the next sections. The structure models were refined using X-ray and neutron powder diffraction data by the Rietveld method implemented in the program Fullprof.⁴⁵ Data collected for samples **s1** were used to refine the structural models of $\text{Pr}^{(11}\text{BD}_4)_3\text{S}(\text{CH}_3)_2$ and $r\text{-Pr}^{(11}\text{BD}_4)_3$, resulting in $R_{\text{wp}} = 6.43$ and 4.66% (not corrected for background), respectively (Fig. S7 and S6†). In order to confirm the crystal structure of $r\text{-Pr}(\text{BH}_4)_3$, and to obtain the exact position of H atoms, $\text{Pr}^{(11}\text{BD}_4)_3$ was synthesized, and NPD of sample **s2** was used to refine the structure model with $R_{\text{wp}} = 3.95\%$ (not corrected for background), $\chi^2 = 4.12$ (Fig. S11†). Moreover, the crystal structure of $\text{Pr}^{(11}\text{BD}_4)_3\text{S}(\text{CH}_3)_2$ was confirmed by Rietveld refinement based on NPD data with $R_{\text{wp}} = 2.00\%$ (not corrected for background), $\chi^2 = 2.18$ (Fig. S9†). NPD data of $\text{Pr}(\text{BD}_4)_3\text{S}(\text{CH}_3)_2$ and $r\text{-Pr}(\text{BD}_4)_3$ were collected from 2θ 10° to 130° ; however, Rietveld refinements of these structures were performed in the 2θ range of 10° to 110° and 10° to 70° , respectively. This was due to the low quality of the neutron diffraction data at high 2θ angles.

The crystal structure of $\beta\text{-Pr}(\text{BH}_4)_3$ and $\beta\text{-Nd}(\text{BH}_4)_3$ was refined based on the XRPD pattern of samples **s3** and **s5** resulting in $R_{\text{wp}} = 2.22\%$ and 4.59% and $\chi^2 = 301$ and 5970 , respectively (see Fig. S5 and S12†). The high χ^2 value is due to extremely high counting statistics of the powder diffraction data obtained from modern 2D detectors. The crystal structures obtained by powder X-ray diffraction were refined based on the fixed positions of the elements in the (known) structure models. Therefore, H–H or D–D distances in these data were obtained by considering the original coordinates of the H/D atoms. The structural model of $\text{Y}(\text{BH}_4)_3$ that was used to refine the structure of the two polymorphs ($Pa\bar{3}$ and $Fm\bar{3}c$) had been optimized by DFT and the H/D coordinates are considered reliable.³⁷ The $R\bar{3}c$ structural model for $\text{La}(\text{BH}_4)_3$ was not optimized by DFT;³⁴ however, the original coordinates of the H/D atoms were used for refinement. In the next step, the H–H/D–D distances were compared to the refinement based on NPD data. In the NPD data refinement, the coordinates of D atoms were refined and for this purpose, additional strains were added to the structures, and B–D and D–D distances were fixed at 1.19 and 1.90 \AA , respectively. The D–D distances obtained by NPD were in agreement with the values obtained by XRPD. The backgrounds were described by linear interpolation between selected points. Unit cell parameters, scale factors, zero-point, peak shape mixing parameters (pseudo-Voigt function), and three profile parameters (U , V , W) were refined. The crystallographic data of the compounds are provided in Table 2.

2.5 Thermal analysis and mass spectrometry

The thermal behavior of the samples was studied by combined thermogravimetric analysis (TGA), differential scanning calorimetry (DSC), and mass spectrometry (MS). DSC and TGA were carried out using a PerkinElmer STA 6000 apparatus, which was attached to a Hiden Analytical HPR-20 QMS mass spectrometer. Approximately 10 mg of the sample was placed in an Al_2O_3 crucible and heated from 40 to $500 \text{ }^\circ\text{C}$ ($\Delta T/\Delta t = 5 \text{ }^\circ\text{C min}^{-1}$) in an argon flow of 40 mL min^{-1} . The evolved gases were transported to a MS and analyzed for H_2 ($m/z = 2$) and B_2H_6 ($m/z = 27$).

2.6 DFT calculations

Quantum Espresso version 6.1⁴⁶ was employed for DFT periodic lattice calculations using the Generalized Gradient Approximation (GGA) functional PW86PBE,^{47,48} with the

Table 1 Overview of investigated samples, molar ratio of the used reactants, synthesis procedure, and the sample composition determined by Rietveld refinement of XRPD or NPD data, the latter indicated by (*)

Sample	Reactants	Molar ratio	Preparation method	Products observed by XRPD/NPD (wt%)
s1	$\text{PrD}_3 - \text{S}(\text{CH}_3)_2^{11}\text{BD}_3$	1 : 4.5	Solvent method	$\text{Pr}^{(11}\text{BD}_4)_3\text{S}(\text{CH}_3)_2$, 91.1(9) $\alpha\text{-Pr}^{(11}\text{BD}_4)_3 - Pa\bar{3}$, 7.4(2) $\beta\text{-Pr}^{(11}\text{BD}_4)_3 - Fm\bar{3}c$, 1.5(1)
s2	$\text{PrD}_3 - \text{S}(\text{CH}_3)_2^{11}\text{BD}_3$	1 : 4.5	Solvent method, $T = 180 \text{ }^\circ\text{C}$, 1 h	$\alpha\text{-Pr}^{(11}\text{BD}_4)_3 - Pa\bar{3}$, 100.0(1)*
s3	$\text{PrH}_3 - \text{S}(\text{CH}_3)_2\text{BH}_3$	1 : 4.5	Solvent method, $T = 180 \text{ }^\circ\text{C}$, 1 h	$\alpha\text{-Pr}(\text{BH}_4)_3 - Pa\bar{3}$, 97.9(2) $\beta\text{-Pr}(\text{BH}_4)_3 - Fm\bar{3}c$, 3.1(3)
s4	$\text{NdH}_3 - \text{S}(\text{CH}_3)_2\text{BH}_3$	1 : 4.5	Solvent method	$\text{Nd}(\text{BH}_4)_3\text{S}(\text{CH}_3)_2$, 100.0(1)
s5	$\text{NdH}_3 - \text{S}(\text{CH}_3)_2\text{BH}_3$	1 : 4.5	Solvent method, $T = 180 \text{ }^\circ\text{C}$, 1 h	$\alpha\text{-Nd}(\text{BH}_4)_3 - Pa\bar{3}$, 93.2(1) $\beta\text{-Nd}(\text{BH}_4)_3 - Fm\bar{3}c$, 6.8(5)

Table 2 Structural data extracted from Rietveld refinements of the XRPD and NPD data for $\text{Pr}(\text{BH}_4)_3\text{S}(\text{CH}_3)_2$, different polymorphs of $\text{Pr}(\text{BH}_4)_3$ and $\beta''\text{-Nd}(\text{BH}_4)_3$

Sample	$\text{Pr}(\text{}^{11}\text{BD}_4)_3\text{S}(\text{CH}_3)_2$	$\alpha\text{-Pr}(\text{BH}_4)_3$	$\beta''\text{-Pr}(\text{BH}_4)_3$	$r\text{-Pr}(\text{}^{11}\text{BD}_4)_3$	$\beta''\text{-Nd}(\text{BH}_4)_3$
Crystal system	Monoclinic	Cubic	Cubic	Trigonal	Cubic
Space group	$P2_1/c$	$Pa\bar{3}$	$Fm\bar{3}c$	$R\bar{3}c$	$Fm\bar{3}c$
T (°C)	RT	RT	190	160	269
$p(\text{Ar}, \text{H}_2)$ (bar)	$p(\text{Ar}) = 1$	$p(\text{Ar}) = 1$	$p(\text{H}_2) = 40$	$p(\text{Ar}) = 1$	$p(\text{H}_2) = 98$
a (Å)	5.6950(2)	11.2941(5)	11.1438(7)	7.373(6)	11.1386(1)
b (Å)	22.9167(1)	—	—	—	—
c (Å)	8.2400(4)	—	—	19.89(2)	—
β (°)	100.68(0)	90	90	120	90
RE–B ^a (Å)	—	2.8607(1)	2.7859(2)	2.8395(16)	2.7847(3)
Z	4	8	8	6	8
V (Å ³)	1056.78(60)	1440.64(11)	1383.88(15)	936.38(14)	1381.95(21)
V/Z (Å ³)	264.2	180.1	172.98	156.1	172.7
ρ (g cm ⁻³)	1.6318	1.7098	1.7801	2.1015	1.8146
ρ_v (H ₂) (kg H ₂ per m ³)	114.0427	111.5413	116.1161	257.1704	116.2783
ρ_m (H ₂) (wt%)	7.3284	6.5226	6.5226	12.2370	6.4074
Radiation	X-ray	X-ray	X-ray	Neutron	X-ray

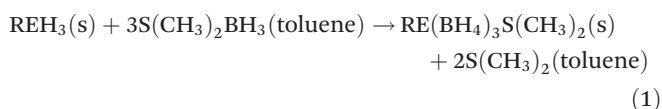
^aPr–B distance for $\alpha\text{-Pr}(\text{BH}_4)_3$ is calculated based on the average of two Pr–B distances in the structure.

inclusion of the exchange-hole dipole moment (XDM) dispersion correction method^{49,50} for modeling weak interactions. XDM dispersion energies were calculated adopting the damping parameters optimized for similar inorganic systems.⁵¹ Cut-offs of 60 Ry were used for structural optimizations. The Brillouin zones were automatically sampled with the Monkhorst–Pack scheme⁵² in a similar approach to that previously described.⁵³ Geometry optimization was performed with a grid mesh of $1 \times 1 \times 2$.

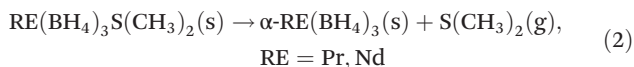
3. Results and discussion

3.1 Synthesis

A new approach to synthesize pure rare-earth metal borohydrides is presented using metal hydrides, REH_3 , RE = Pr, Nd, and a borane donating complex, $\text{S}(\text{CH}_3)_2\text{BH}_3$ in solution, forming solvated complexes, see reaction (1).



Using this method, $\text{Pr}(\text{BH}_4)_3\text{S}(\text{CH}_3)_2$ and $\text{Nd}(\text{BH}_4)_3\text{S}(\text{CH}_3)_2$ are synthesized and $\text{Pr}(\text{BH}_4)_3$ and $\text{Nd}(\text{BH}_4)_3$ are obtained by heating the solvate complexes under vacuum at 180 °C, see reaction (2).



$\text{Pr}(\text{}^{11}\text{BD}_4)_3\text{S}(\text{CH}_3)_2$ and $\text{Pr}(\text{}^{11}\text{BD}_4)_3$ were synthesized using a similar approach, reaction (1) and (2), and PrD_3 and $\text{S}(\text{CH}_3)_2\text{}^{11}\text{BD}_3$ as reactants.

3.2. Structure analysis

3.2.1. Crystal structure of $\text{RE}(\text{BH}_4)_3\text{S}(\text{CH}_3)_2$, RE = Pr, Nd. The diffraction patterns of the praseodymium(III) and neo-

dymium(III) borohydride dimethyl sulfide complex, $\text{RE}(\text{BH}_4)_3\text{S}(\text{CH}_3)_2$, RE = Pr, Nd clearly resembled the Bragg reflections of $\text{Y}(\text{BH}_4)_3\text{S}(\text{CH}_3)_2$ and $\text{Gd}(\text{BH}_4)_3\text{S}(\text{CH}_3)_2$.³⁶ Therefore, the $\text{Y}(\text{BH}_4)_3\text{S}(\text{CH}_3)_2$ structure (monoclinic, $P2_1/c$) was used as an initial structural model for Rietveld refinements, see Table 2. In this structure, the rare-earth cation is coordinated to five BH_4^- units and a sulfur atom from the dimethyl sulfide molecule, forming a distorted octahedral geometry. Four BH_4^- groups bridge between the RE^{3+} centers by edge sharing, bidentate (η^2) coordination, and the remaining BH_4^- group is a terminal ligand. The $\text{S}(\text{CH}_3)_2$ molecule coordinates to RE^{3+} via the S atom of $\text{S}(\text{CH}_3)_2$ (Fig. 1). The structure of $\text{Pr}(\text{}^{11}\text{BD}_4)_3\text{S}(\text{CH}_3)_2$ was refined using the Rietveld method using both X-ray and neutron powder diffraction data, Fig. S7 and S8.† The refined structural data are provided in Table 2.

3.2.2 Crystal structure of $\alpha\text{-RE}(\text{BH}_4)_3$. The room temperature polymorphs of praseodymium(III) and neodymium(III) borohydrides, $\alpha\text{-RE}(\text{BH}_4)_3$, RE = Pr, Nd, crystallize in space group

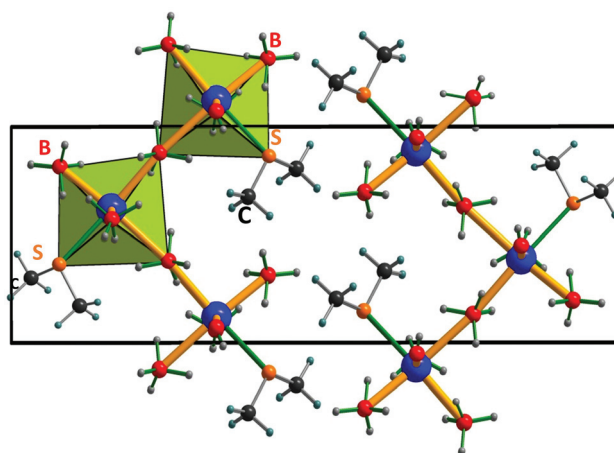


Fig. 1 Crystal structure of $\text{Pr}(\text{}^{11}\text{BD}_4)_3\text{S}(\text{CH}_3)_2$ and $\text{Nd}(\text{BH}_4)_3\text{S}(\text{CH}_3)_2$.

$Pa\bar{3}$ and are isostructural to RT polymorphs of α -Y(BH₄)₃ and α -Gd(BH₄)₃.^{20,36,38} The rare-earth atoms coordinate to six BH₄⁻ units with two different RE–B distances, *i.e.* Pr–B of 2.8535(1) and 2.8679(1) Å, and Nd–B of 2.8306(1) and 2.8449(1) Å, respectively, forming a distorted octahedral geometry. BH₄⁻ complexes bridge the RE³⁺ centers with bidentate (η^2) coordination resulting in a 12-fold coordination of RE to hydrogen (Fig. 2, middle).

3.2.3 Crystal structure of β -RE(BH₄)₃. Two different space groups of $Fm\bar{3}c$ and $Pm\bar{3}m$ have been reported for β -RE(BH₄)₃ as a high-temperature polymorph. The $Fm\bar{3}c$ structure has a

fully ordered array of [BH₄]⁻ groups, with 8 formula units in the unit cell, while the $Pm\bar{3}m$ structure has half the lattice parameter and the unit cell contains one formula unit.^{20,37,38} The BH₄⁻ complexes randomly take either of the two possible orientations in the $Pm\bar{3}m$ structure. The X-ray diffraction patterns of these two structural models are similar and cannot be distinguished. However, neutron powder diffraction of Y(BH₄)₃ has shown that the $Fm\bar{3}c$ structure is the correct space group.^{37,38}

High temperature polymorphs, β -RE(BH₄)₃, RE = Pr, Nd ($Fm\bar{3}c$), are formed when α -RE(BH₄)₃ is heated under high hydrogen pressures. The β - polymorphs are isostructural to β -RE(BH₄)₃, RE = Ce, Sm, Ho, Y, Er, Tm, Yb, with straight RE–BH₄–RE coordination (η^2), which is isostructural to the ideal cubic ReO₃ structure (Fig. 2, bottom). The RE atoms coordinate to six BH₄⁻ units with the same distance of Pr–B = 2.7859(2) Å (T = 190 °C) and Nd–B = 2.7847(3) Å (T = 269 °C), forming an ideal octahedral geometry in comparison with the distorted octahedron observed for the α -RE(BH₄)₃.³⁷ The β - polymorphs also have a bidentate (η^2) coordination of RE to BH₄⁻ forming a 12-fold coordination of RE to hydrogen. This structure contains large unoccupied voids at ($\frac{1}{4}, \frac{1}{4}, \frac{1}{4}$) coordinate with a distance of ~ 3.35 Å from the center to the nearest hydrogen atom (Fig. 2, bottom).³⁴

3.2.4 Crystal structure of r -RE(BH₄)₃. A rhombohedral deformation of cubic β -Pr(BH₄)₃, denoted as r -RE(BH₄)₃, that crystallizes in the trigonal crystal system with space group $R\bar{3}c$ (Z = 6) is also observed, which is isostructural to a high-pressure polymorph of rhenium trioxide, ReO₃.⁵⁴ r -RE(BH₄)₃ has been observed as the room temperature polymorph for RE = La, Ce. However, r -Pr(BH₄)₃ forms at T > 190 °C and the structure has been confirmed by Rietveld refinement of NPD data of r -Pr(¹¹BD₄)₃ (Fig. S11†). Six BH₄⁻ complexes are coordinated to each Pr³⁺ ion forming a regular octahedra, Pr–B distance of 2.8395(16) Å, similar to that observed in β -Pr(BH₄)₃.

3.2.5 DFT optimization of the Pr(BH₄)₃ polymorphs. Period plane wave DFT calculations of the three polymorphs were attempted in order to shed light on their properties. The structure of α -Pr(BH₄)₃, (the $Pa\bar{3}$ form), has been fully optimized with no constraints (128 atoms; for this large cell, Z = 8, a Monkhorst–Pack grid of $1 \times 1 \times 1$ was selected). The calculations were performed adopting an antiferromagnetic structure, in which half of the Pr atoms have positive magnetization and half negative, with a total magnetization equal to zero. Calculations with different magnetization schemes failed to converge. By this approach, the optimized cell volume is larger than the experimental one by only 1.27%, and final geometry and ion positions in the cell are very similar to the starting one. Similar calculations on the $Fm\bar{3}c$ and the $R\bar{3}c$ structures resulted in a significantly larger unit cell, +12.3% and +20.5%, respectively. The overestimation of the unit cell size is likely due to neglecting phonon interactions, which become significant at higher temperatures required to convert Pr(BH₄)₃ to the $Fm\bar{3}c$ and $R\bar{3}c$ polymorphs. Therefore, a simplified approach was adopted, which allows comparing the energy of the three

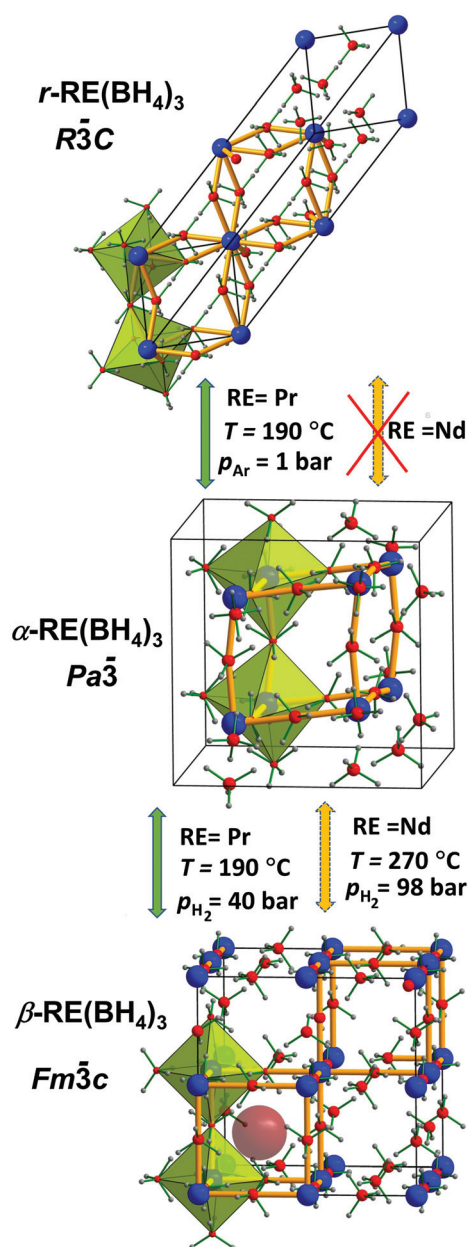


Fig. 2 Crystal structures of (top) r -Pr(BH₄)₃, $R\bar{3}c$, (middle) α -RE(BH₄)₃, $Pa\bar{3}$, and (bottom) β -RE(BH₄)₃, $Fm\bar{3}c$. One of the empty voids in the β -Pr(BH₄)₃ structure is shown with a reddish/violet sphere.

different structures: only the atom positions within the unit cell were optimized with unit cell parameters fixed to the experimental values. By this method, the $Pa\bar{3}$ structure computed by DFT is the most stable, with the $Fm\bar{3}c$ and the $R\bar{3}c$ higher in energy by 4.3 and 6.4 kcal mol⁻¹, respectively, corresponding to decreasing stability of α -Pr(BH₄)₃ > β -Pr(BH₄)₃ > r -Pr(BH₄)₃. Moreover, DFT calculations of the r -Pr(¹¹BD₄)₃ structure obtained by NPD and with fixed unit cell parameters show 7.4 kcal mol⁻¹ higher energy than that of the $Pa\bar{3}$ structure. However, this relative energy order could be easily modified at higher temperatures, because the energy values of the three structures are close to each other.

3.3 *In situ* synchrotron radiation X-ray powder diffraction

3.3.1 Investigation of Pr(BH₄)₃ polymorphism as a function of p, T . The thermal properties of Pr(¹¹BD₄)₃S(CH₃)₂ in $p(\text{Ar}) = 1$ bar are investigated by *in situ* SR-XRPD, see Fig. 3. Only the Bragg reflections of the solvate compound are observed at RT. At $T > 130$ °C, Pr(¹¹BD₄)₃S(CH₃)₂ decomposes with the release of S(CH₃)₂, and formation of two different polymorphs of praseodymium(III) borohydride, α - and β -Pr(¹¹BD₄)₃, 66.8(3) and 33.2(3) wt%, respectively (Fig. S1†). Further heating of the sample leads to a decreasing degree of the long range order of the β polymorphs (*i.e.* decreasing diffracted intensity of β) and an apparent increasing amount of α -Pr(¹¹BD₄)₃. This occurs because the sample composition is normalized to 1 (notice that the diffracted intensity of α appears constant in the temperature range of ~150 to ~180 °C). The Bragg reflections of β -Pr(¹¹BD₄)₃ are abruptly shifted to higher 2θ angles at ~176 °C with a similar abrupt increase of the diffracted intensity, revealing a contraction of the unit cell and the formation of a new polymorph denoted as β' -Pr(BH₄)₃ ($Fm\bar{3}c$) (not shown in Fig. 3b because of the overlap of the Bragg reflections of α and β' phases at $2\theta = 7.2^\circ$ and 10.2°). At the same time, the fraction of this polymorph, β' , increases and reaches a maximum of 33.5(9) wt% at 185 °C (Fig. 3b). At $T = 190$ °C, α -Pr(¹¹BD₄)₃ disappears, and r -Pr(¹¹BD₄)₃ with the smallest V/Z forming as the major polymorph, 89(1) wt%. Simultaneously, the unit cell volume of β' -Pr(¹¹BD₄)₃ shrinks for the second time to $V/Z \sim 170.9$ Å³, forming a polymorph denoted as β'' -Pr(¹¹BD₄)₃ (displayed by arrows in Fig. 3a). The structural mechanism for formation of the four polymorphs of praseodymium(III) borohydride is discussed in section 3.5.

Upon cooling, the polymorphs r - and β'' -Pr(¹¹BD₄)₃ are stable at 119 °C where α -Pr(¹¹BD₄)₃ starts to form at the expense of r -Pr(¹¹BD₄)₃. Further cooling of the sample fully transforms the r -Pr(¹¹BD₄)₃ to α -Pr(¹¹BD₄)₃ and the sample composition at 59 °C is α -Pr(¹¹BD₄)₃ 83(1) wt% and β'' -Pr(¹¹BD₄)₃ 17.5(7) wt%. The *in situ* SR-XRPD data of Pr(BH₄)₃ heated under $p(\text{Ar}) = 1$ bar (see Fig. S2†) are similar to those presented in Fig. 3 of Pr(¹¹BD₄)₃S(CH₃)₂.

A second series of *in situ* XRPD experiments were performed under a hydrogen atmosphere, $p(\text{H}_2) = 40$ bar, in order to investigate the possible effect of gas and partial pressure on the structural evolution, and the data are presented in Fig. 4a and S3.† *In situ* SR-XRPD of Pr(BH₄)₃ at RT reveals diffractions

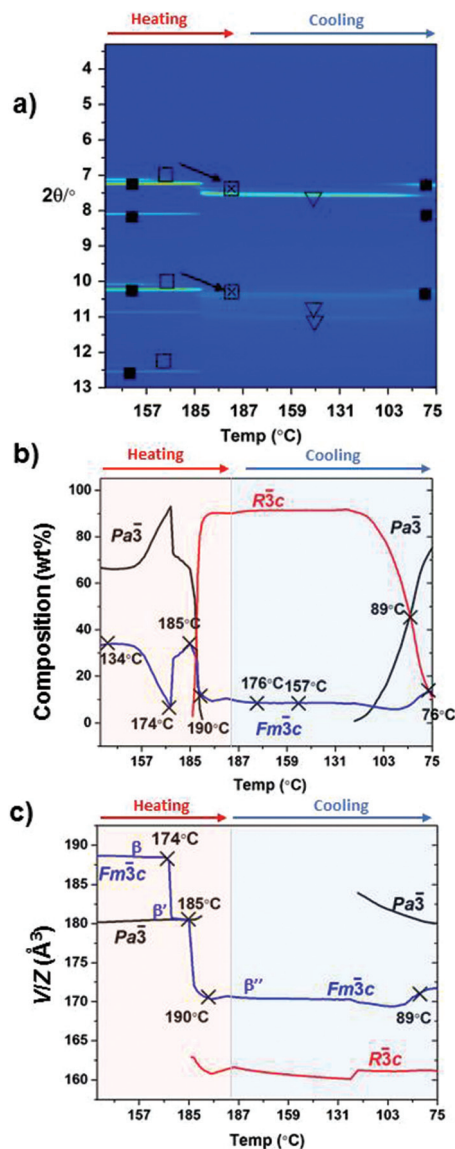


Fig. 3 (a) *In situ* SR-XRPD data of the Pr(¹¹BD₄)₃S(CH₃)₂ compound under $p(\text{Ar}) = 1$ bar. $\Delta T/\Delta t = 5$ °C min⁻¹ ($\lambda = 0.7129$ Å). Symbols: ● Pr(¹¹BD₄)₃S(CH₃)₂; ■ α -Pr(¹¹BD₄)₃ $Pa\bar{3}$; □ β -Pr(¹¹BD₄)₃ $Fm\bar{3}c$; ▲ β' -Pr(¹¹BD₄)₃ $Fm\bar{3}c$ and ▼ for r -Pr(¹¹BD₄)₃ $R\bar{3}c$; (b) Sample composition and (c) V/Z of each polymorph extracted by Rietveld refinement of the SR-XRPD data.

from the polymorphs α - (94.7(3) wt%) and β -Pr(BH₄)₃ (5.3(2) wt%), see Fig. 4b. Prior to this experiment, Pr(BH₄)₃ has been annealed at 180 °C and the observed sample composition is similar to the one observed in the previous experiment at 174 °C using Pr(¹¹BD₄)₃S(CH₃)₂ (Fig. 3b). An abrupt displacement of the β -Pr(BH₄)₃ Bragg reflections towards lower 2θ angles is also observed in this case, at 174 °C, and is assigned to the formation of β' -Pr(BH₄)₃. Moreover, the unit cell volume of β' -Pr(BH₄)₃ shrinks for the second time upon formation of β'' -Pr(BH₄)₃. However, it is noteworthy that β'' -Pr(BH₄)₃, 66.6(8) wt%, is now the main component in the sample at 190 °C. The stabilization of the cubic and porous β'' -Pr(BH₄)₃ in larger

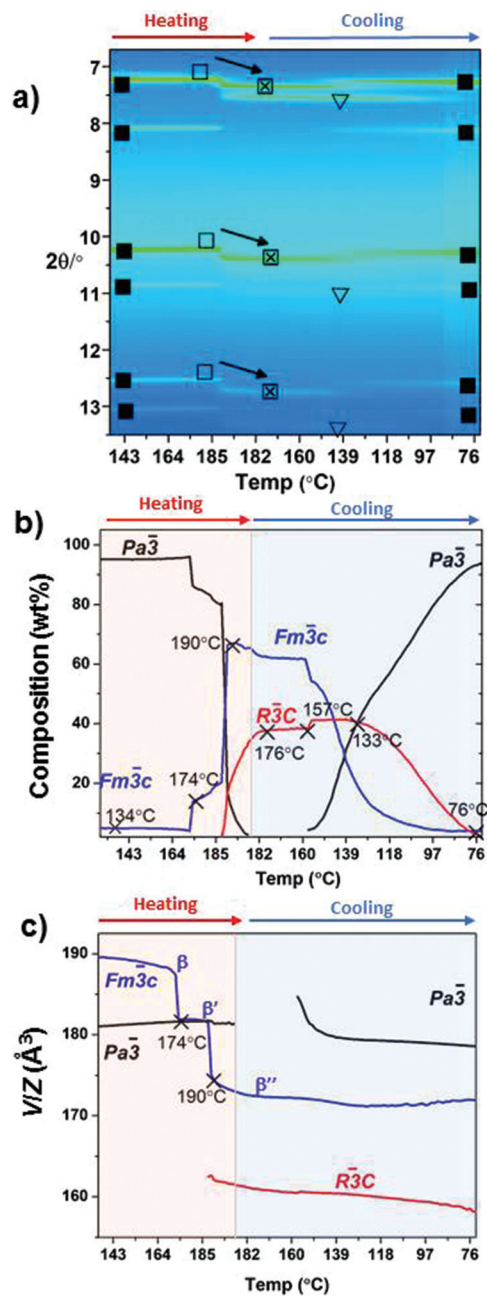


Fig. 4 (a) *In situ* SR-XRPD data of Pr(BH₄)₃ compound under $p(\text{H}_2) = 40$ bar. $\Delta T/\Delta t = 5^\circ\text{C min}^{-1}$ ($\lambda = 0.7129 \text{ \AA}$), symbols: ■ $\alpha\text{-Pr}(\text{BH}_4)_3$ $\text{Pa}\bar{3}$; □ $\beta\text{-Pr}(\text{BH}_4)_3$ $\text{Fm}\bar{3}c$; ◀ $\beta'\text{-Pr}(\text{BH}_4)_3$ $\text{Fm}\bar{3}c$ and ▽ for $r\text{-Pr}(\text{BH}_4)_3$ $\text{R}\bar{3}c$; (b) Sample composition and (c) V/Z of each polymorph extracted by Rietveld refinement of SR-XRPD data.

amounts here contrasts the formation of $r\text{-Pr}(\text{BH}_4)_3$, 89(1) wt%, at 190 °C, in the previous measurement (Fig. 3b). At $T = 190^\circ\text{C}$, the Bragg reflections of $\alpha\text{-Pr}(\text{BH}_4)_3$ disappear and $r\text{-Pr}(\text{BH}_4)_3$ forms in smaller amounts. This clearly shows the strong influence of gas and partial pressures on the polymorphism of Pr(BH₄)₃. Upon cooling, $\beta''\text{-Pr}(\text{BH}_4)_3$ remains as the major polymorph at 157 °C where transformation to $\alpha\text{-Pr}(\text{BH}_4)_3$ starts.

The extracted unit cell volumes (V/Z) as a function of temperature (Fig. 4c) show that the $\beta''\text{-Pr}(\text{BH}_4)_3$ structure is $\sim 10 \text{ \AA}^3$ more expanded as compared to that of $r\text{-Pr}(\text{BH}_4)_3$ upon cooling in the temperature range of 190 to $\sim 100^\circ\text{C}$, for both experiments (Fig. 3c and 4c).

3.3.2 Investigation of Nd(BH₄)₃ polymorphism as a function of p, T . The neodymium borohydride solvate, Nd(BD₄)₃S(CH₃)₂ (**s4**), was also investigated by *in situ* SR-XRPD under $p(\text{Ar}) = 1$ bar, see Fig. S3,† and Bragg reflections of this compound are observed in the temperature range of RT to 165 °C. Nd(BD₄)₃S(CH₃)₂ decomposes with release of S(CH₃)₂ and formation of $\alpha\text{-Nd}(\text{BD}_4)_3$, at $T > 165^\circ\text{C}$. However, no polymorphic transitions are observed for Nd(BH₄)₃ by further heating, and the sample starts to decompose at $T \sim 213^\circ\text{C}$.

In situ SR-XRPD of Nd(BH₄)₃ under $p(\text{H}_2) = 98$ bar has also been measured, see Fig. S4.† At RT, the sample contains $\alpha\text{-Nd}(\text{BH}_4)_3$, 93(1) wt%, and $\beta\text{-Nd}(\text{BH}_4)_3$, 6.8(5) wt%. Similar to Pr(BH₄)₃, when the sample is heated under hydrogen pressure, a stepwise polymorphic transition is observed $\beta \rightarrow \beta' \rightarrow \beta''\text{-Nd}(\text{BH}_4)_3$, *i.e.* another rare example of negative thermal expansion. This sample fully transforms to $\beta''\text{-Nd}(\text{BH}_4)_3$ at 270 °C, which is in contrast to the formation of only 66.6(8) wt% of $\beta''\text{-Pr}(\text{BH}_4)_3$ in the previous experiment. These polymorphic transitions are reversible, and Bragg reflections of $\alpha\text{-Nd}(\text{BH}_4)_3$ start to appear upon cooling at $T \sim 230^\circ\text{C}$. The observation of the polymorphic transition at higher temperatures for Nd(BH₄)₃ ($T = 270^\circ\text{C}$) and the suppression of decomposition are clearly due to the elevated hydrogen pressure used in this experiment.

3.4 Atomic distances of praseodymium(III) borohydride as a function of p, T

The Pr–B distances and weight fractions of praseodymium(III) borohydride polymorphs obtained from Rietveld refinements of *in situ* SR-XRPD data at $p(\text{Ar}) = 1$ bar and selected temperatures are shown in Fig. 5. The $\alpha\text{-Pr}(\text{BD}_4)_3$ polymorph (67.8(3) wt%) has a Pr–B distance of 2.8611(1) Å, at $T = 134^\circ\text{C}$. The major component at 190 °C, $r\text{-Pr}(\text{BD}_4)_3$ (95(2) wt%) has a longer Pr–B distance of 2.9236(4) Å due to transverse rotation of Pr(BD₄)₆ octahedra. In this process, the B atom in the middle of the Pr–B–Pr linkage is displaced transversely, the Pr–B distance is increased, and the two Pr atoms are pulled together, inducing a contraction in the unit cell volume. Upon cooling to 76 °C, $\alpha\text{-Pr}(\text{BD}_4)_3$ (73(1) wt%) forms with a shorter Pr–B distance of 2.8606(1) Å as compared to the r -polymorph.

The Pr–B distances of the different polymorphs of Pr(BH₄)₃ during heat treatment under $p(\text{H}_2) = 40$ bar are shown in Fig. 6. At 134 °C, $\alpha\text{-Pr}(\text{BH}_4)_3$, 88.7(5) wt%, is the dominant polymorph with Pr–B distances of 2.8654(1) Å. Increasing the temperature facilitates the formation of the β -polymorphs with distinct Pr–B distances of 2.8726(1), 2.8321(2) and 2.7859(2) Å for β -, β' - and β'' - measured at 134, 185 and 190 °C, respectively.

These results reveal that the type of gas (Ar or H₂) and partial pressures influence the Pr–B bond lengths. When experiments are performed in $p(\text{Ar}) = 1$ bar, complete rotation

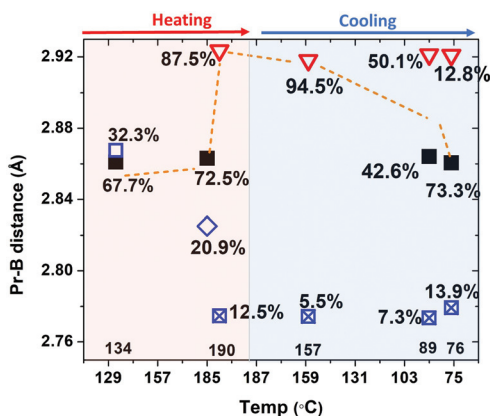


Fig. 5 Pr–B distances of each Pr(BH₄)₃ polymorph at different temperatures under $p(\text{Ar}) = 1$ bar obtained by Rietveld refinement of XRPD data (Fig. 3a). The weight percent of the polymorphs at each temperature is written in the figures. The dashed line connects the polymorphs with the highest amount (wt%) at each temperature. Symbols: ■ α -Pr(BH₄)₃ $Pa\bar{3}$; □ β -Pr(BH₄)₃ $Fm\bar{3}c$; ◇ β' -Pr(BH₄)₃ $Fm\bar{3}c$; ◀ β'' -Pr(BH₄)₃ $Fm\bar{3}c$ and ▽ for r -Pr(BH₄)₃ $R\bar{3}c$.

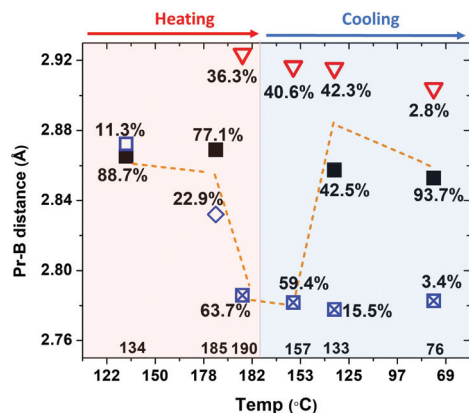


Fig. 6 Pr–B distances of each Pr(BH₄)₃ polymorph at different temperatures under $p(\text{H}_2) = 40$ bar obtained by Rietveld refinement of XRPD data (Fig. 4a). The sample composition (wt%) at each temperature is given in the figure with a dashed line connecting the polymorphs with the highest amount. Symbols: ■ α -Pr(BH₄)₃ $Pa\bar{3}$; □ β -Pr(BH₄)₃ $Fm\bar{3}c$; ◇ β' -Pr(BH₄)₃ $Fm\bar{3}c$; ◀ β'' -Pr(BH₄)₃ $Fm\bar{3}c$ and ▽ for r -Pr(BH₄)₃ $R\bar{3}c$.

of Pr(BH₄)₆ octahedra occurs and r -Pr(BH₄)₃ with a longer Pr–B distance forms. However, in $p(\text{H}_2) = 40$ bar, the porous β polymorphs stabilize with straight Pr–BH₄–Pr coordination and shorter Pr–B distances.

3.5 Mechanism for transformation of praseodymium(III) borohydride polymorphs

The three polymorphs α -, β - and r -Pr(BH₄)₃, have the rhenium(VI) trioxide, ReO₃, structure types. In an ideal cubic ReO₃ structure, the Re atoms occupy the corners of the cube and coordinate to six oxygen atoms placed on the centers of the edges. This is also the case for the cubic β -Pr(BH₄)₃ with Pr–B–Pr bond angles of 180°. This structure type is closely related to

the perovskite structure, *i.e.* SrTiO₃, but without the Sr atoms located on the center of the cube leaving an empty void in this position (see Fig. 2).⁵⁵

A wide variety of crystal structures can be derived by coupled rotation of octahedra, *i.e.* [RE(BH₄)₆], without breaking or forming chemical bonds, such as α - and r -Pr(BH₄)₃, which crystallize in distorted ReO₃ structures. At RT, α -Pr(BH₄)₃ is stable, which unfolds to the ideal ReO₃ structure, β -Pr(BH₄)₃, upon heating, but this polymorph is unstable and transforms to r -Pr(BH₄)₃ (Fig. 7). The transformation of the β

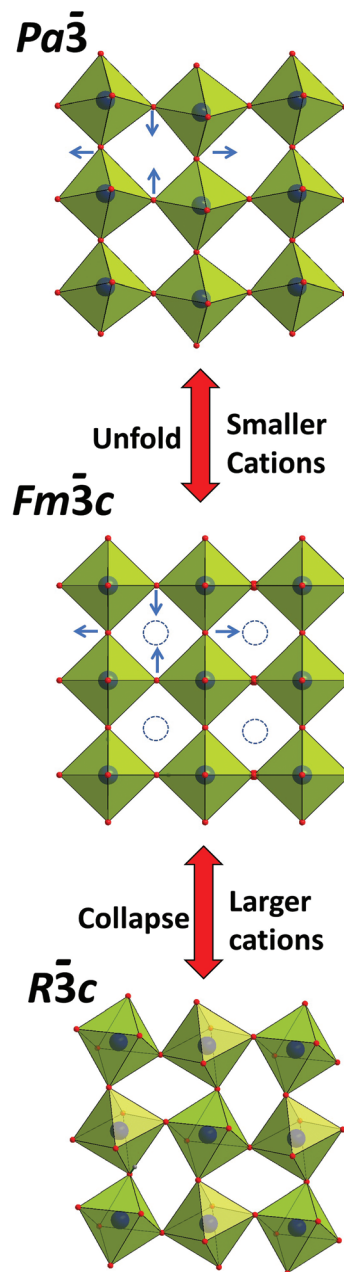


Fig. 7 The REB₆ polyhedra in space group symmetries $Pa\bar{3}$, $Fm\bar{3}c$ and $R\bar{3}c$. The empty voids in the $Fm\bar{3}c$ structure are presented by (blue dashed) empty circles.

to *r*-polymorph is assigned to the large voids in the β -polymorph that allow bending of the Pr–B–Pr linkage, which increases the Pr–B bond distance, decrease the Pr–Pr distance by rotation of $\text{Pr}(\text{BH}_4)_6$ octahedra and consequently contract the unit cell volume. The transformation of β - to *r*- $\text{Pr}(\text{BH}_4)_3$ occurs *via* two other polymorphs, β' - and β'' - $\text{Pr}(\text{BH}_4)_3$ as further discussed below. The polymorphs β - and *r*- $\text{Pr}(\text{BH}_4)_3$ are only stable at elevated temperatures and transform back to α - $\text{Pr}(\text{BH}_4)_3$ at RT, possibly due to H–H repulsion.

The relationship between hexagonal (*r*) and cubic (β) unit cell parameters in an ideal cubic crystal system is $a(r) = \frac{a(\beta)\sqrt{2}}{2}$ and $c(r) = a(\beta)\sqrt{3}$. The values determined from the Rietveld refinement of *r*- and β'' - $\text{Pr}(\text{BH}_4)_3$ at 190 °C are $a(r) = 7.4831(12)$, $c(r) = 19.995(5)$ and $a(\beta'') = 11.1438(7)$ Å, respectively. Therefore, the calculation of the non-deformed hexagonal unit cell from the cubic cell is $a(r) = \frac{11.1438\sqrt{2}}{2} = 7.8798$ Å and $c(r) = 11.1314\sqrt{3} = 19.3016$ Å. This shows that the rhombohedral structure is compressed along $a(r)$ and expanded along $c(r)$. The same deformation has been observed for $\text{Ce}(\text{BH}_4)_3$ and $\text{La}(\text{BH}_4)_3$ polymorphs.³⁴

The cubic to rhombohedral β - to *r*- $\text{Pr}(\text{BH}_4)_3$ transformation deserves more attention. This transformation clearly occurs *via* two intermediate polymorphs, β' - and β'' - $\text{Pr}(\text{BH}_4)_3$, with distinct unit cell differences as illustrated in Fig. 3c and 4c. The extracted unit cell volumes (V/Z) as a function of temperature reveal a stepwise decrease of ~ 8 – 10 Å³ per transformation in the series: $\beta \rightarrow \beta' \rightarrow \beta'' \rightarrow r\text{-Pr}(\text{BH}_4)_3$. The V/Z values suggest that $\sim 1/3$ and $\sim 2/3$ of the original cubic structure is contracted to the rhombohedral structure type in β' - and β'' - $\text{Pr}(\text{BH}_4)_3$ ($p(\text{H}_2) = 40$ bar). This may suggest static disorder created by rotation of $[\text{Pr}(\text{BH}_4)_6]$ octahedra, which reduces the Pr–Pr distance and results in a decrease in the unit cell volume. A dynamic effect, such as transverse vibration of BH_4 complexes normal to the Pr–Pr axis or rotation around this axis, is an alternative explanation. However, this is expected to provide a continuous change of unit cell volume as a function of temperature, which contrasts the stepwise changes clearly observed in Fig. 3c and 4c.

A similar behaviour has also been observed for ScF_3 with an identical cubic ReO_3 structure type responsible for negative thermal expansion (NTE) and zero thermal expansion (ZTE) of $(\text{Sc}_{0.85}\text{Ga}_{0.05}\text{Fe}_{0.1})\text{F}_3$.^{56,57} However, unlike $\text{Pr}(\text{BH}_4)_3$, continuous contraction of the unit cell volume is observed for ScF_3 . For these fluorides, the collapse in the unit cell volume upon heating is attributed to the partial formation of a rhombohedral structure in a cubic-like form rather than a rhombohedral unit cell. In this case, the long-range structure remains cubic, but the local structure is distorted in a similar way to that in the rhombohedral polymorph, which makes it very challenging to identify by XRPD. This occurs due to transverse vibration of fluoride anions, *i.e.* a dynamic effect.⁵⁶

We observe that ~ 95 wt% of $\text{Pr}(\text{BH}_4)_3$ transforms completely to the rhombohedral polymorph upon heating in argon, $p(\text{Ar}) = 1$ bar, *i.e.* the structure becomes rhombohedral both

locally and over a long range. However, a minor amount keeps the cubic long range order and shows a stepwise decrease of the unit cell volume, *i.e.* β' - (20 wt% at 185 °C) and β'' - $\text{Pr}(\text{BH}_4)_3$ (5 wt% at 190 °C). Hydrogen gas, $p(\text{H}_2) = 40$ bar, clearly facilitates the stepwise polymorphic transitions $\beta \rightarrow \beta' \rightarrow \beta'' \rightarrow \alpha\text{-Pr}(\text{BH}_4)_3$ upon heating/cooling of ~ 65 wt% of the sample. A similar trend is observed for neodymium(III) borohydride with no observation of β -polymorphs in $p(\text{Ar}) = 1$ bar but increasing amount in $p(\text{H}_2) = 40$ bar, *i.e.* 7.9(6), 20.8(9) and 100 wt% of $\beta \rightarrow \beta' \rightarrow \beta''\text{-Nd}(\text{BH}_4)_3$, at 134, 190 and 270 °C.

3.6 Comparison of the crystal structures of the different RE $(\text{BH}_4)_3$ compounds

The series of rare earth borohydrides show significant structural changes as a function of small changes in the cation ionic radii. The largest rare-earth metal borohydrides, La and Ce, crystallize as the polymorph *r*- $\text{RE}(\text{BH}_4)_3$ at RT and have smaller unit cell volumes and higher densities compared to the cubic structure type, $\alpha\text{-RE}(\text{BH}_4)_3$. The smaller RE elements crystallize in cubic structures, *e.g.* as $\alpha\text{-Pr}(\text{BH}_4)_3$. This work highlights praseodymium as a ‘border line’ RE element, which exists in five different polymorphs α -, β -, β' -, β'' -, and *r*- $\text{Pr}(\text{BH}_4)_3$. This trend, presented in Fig. 8, suggests that the crystal structures of the rare-earth metal borohydrides are dependent on the size of the cation.

Previous experiments have shown that $\beta\text{-Ce}(\text{BH}_4)_3$ is only formed when $\text{Ce}(\text{BH}_4)_3\text{S}(\text{CH}_3)_2$ is heated in a closed capillary, and that annealing under dynamic vacuum forms the *r*-polymorph. Our experimental work reveals that formation of $\beta\text{-Pr}(\text{BH}_4)_3$ and two intermediate polymorphs, β' - and $\beta''\text{-Pr}(\text{BH}_4)_3$, can be facilitated by $p(\text{H}_2) = 40$ bar and $T = 175$ and 190 °C, respectively. Thus, the presence of gasses clearly facilitates stabilization of the β -polymorphs.

The radius of the neodymium ion is slightly smaller as compared to that of praseodymium, $r(\text{Nd}^{3+}) = 1.123$ and $r(\text{Pr}^{3+})$

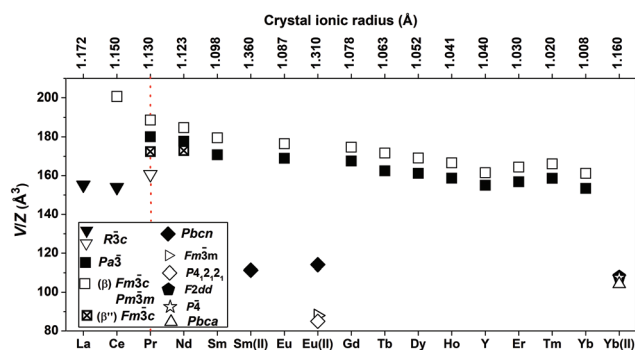


Fig. 8 Unit cell volumes (V) divided by the number of formula units (Z) of the reported rare-earth borohydrides. β polymorphs of $\text{Pr}(\text{BH}_4)_3$ and $\text{Nd}(\text{BH}_4)_3$ polymorphs are recorded at RT, while β'' polymorphs are recorded at 190 and 269 °C, respectively. β' polymorphs of $\text{Pr}(\text{BH}_4)_3$ and $\text{Nd}(\text{BH}_4)_3$ are not shown in this figure but their structural data are presented in Tables s1–s3.[†] The ionic radii are taken from ref. 58. Polymorphs stable at RT are shown with a filled symbol (■). Space groups of $Fm\bar{3}c$ and $Pm\bar{3}m$ are presented by one symbol (□) because of the similarity of their structures.

$= 1.130 \text{ \AA}$,⁵⁸ and a different polymorphism of $\text{Nd}(\text{BH}_4)_3$ is discovered in this study. No polymorphic changes are observed during heating of $\alpha\text{-Nd}(\text{BH}_4)_3$ in argon; however, $\beta''\text{-Nd}(\text{BH}_4)_3$ forms when heated in hydrogen ($p(\text{H}_2) = 98 \text{ bar}$) and at $T = 270 \text{ }^\circ\text{C}$.

3.7 Thermal analysis

Thermal analysis, TGA-DSC-MS, of $\text{Pr}(\text{BH}_4)_3$ (s3), Fig. 9, reveals a total release of hydrogen of 4.8 wt%, which is lower than the calculated hydrogen content of 5.97 wt% according to the reaction scheme:



Two endothermic peaks are observed in the DSC data, one at $204 \text{ }^\circ\text{C}$ is assigned to the first order polymorphic transition of $\alpha\text{-Pr}(\text{BH}_4)_3$ to $r\text{-Pr}(\text{BH}_4)_3$ and the second at $247 \text{ }^\circ\text{C}$ to the decomposition of the sample. In order to investigate the reversibility of the polymorphic transition, a second experiment

was conducted by heating the sample to $220 \text{ }^\circ\text{C}$ and cooling back to RT. Fig. 9b shows that the sample releases $\sim 0.5 \text{ wt\%}$ of hydrogen during the α to r -polymorphic transition temperature. Upon cooling the sample to RT, an exothermic peak is observed in the DSC curve at $125 \text{ }^\circ\text{C}$. This event is attributed to the polymorphic transition of r - to $\alpha\text{-Pr}(\text{BH}_4)_3$ and is in good agreement with the reformation of $\alpha\text{-Pr}(\text{BH}_4)_3$ at $119 \text{ }^\circ\text{C}$ observed by the *in situ* SR-XRPD experiment.

Thermal analysis, TGA-DSC-MS, of $\text{Nd}(\text{BH}_4)_3$ is shown in Fig. S14,[†] and reveals one endothermic peak in the DSC data, at $T \sim 250 \text{ }^\circ\text{C}$, assigned to decomposition. A release of 5.5 wt% of hydrogen is observed in the temperature range 200 to $400 \text{ }^\circ\text{C}$, which is slightly lower than the calculated hydrogen content, 5.87 wt% based on the reaction:



4. Conclusion

In this study, $\text{Pr}(\text{BD}_4)_3\text{S}(\text{CH}_3)_2$ and four new polymorphs r - and β -, β' - and $\beta''\text{-Pr}(\text{BH}_4)_3$ are presented, which highlights $\text{Pr}(\text{BH}_4)_3$ as a 'border-line' rare earth metal borohydride with unique crystal chemistry. At RT, $\alpha\text{-Pr}(\text{BH}_4)_3$ ($P63$) is formed, and at $T = 190 \text{ }^\circ\text{C}$ the structure transforms to the more dense polymorph $r\text{-Pr}(\text{BH}_4)_3$ ($R3c$). The cubic (β) to rhombohedral, $r\text{-Pr}(\text{BH}_4)_3$ transformation occurs *via* two intermediate polymorphs, β' - and $\beta''\text{-Pr}(\text{BH}_4)_3$, with a distinct decrease of unit cell volumes, and is a rare example of stepwise negative thermal expansion. This suggests static disorder created by rotation of $[\text{Pr}(\text{BH}_4)_6]$ octahedra, which reduces the Pr-Pr distance and results in a decrease in the unit cell volume. A similar, but continuous, change of volume is observed for the isostructural $\text{Sc}(\text{BH}_4)_3$ with the same cubic ReO_3 structure type responsible for negative thermal expansion (NTE) due to a dynamic structural effect.

We observe that $\sim 95 \text{ wt\%}$ of $\text{Pr}(\text{BH}_4)_3$ transforms completely to the rhombohedral polymorph upon heating in argon ($p(\text{Ar}) = 1 \text{ bar}$), *i.e.* the structure becomes rhombohedral both locally and over a long range. However, a minor amount, $\sim 5 \text{ wt\%}$, of $\text{Pr}(\text{BH}_4)_3$ keeps the cubic long range order and shows a stepwise decrease of the unit cell volume. Hydrogen gas ($p(\text{H}_2) = 40 \text{ bar}$) clearly facilitates the stepwise polymorphic transitions $\alpha\text{-Pr}(\text{BH}_4)_3 \rightarrow \beta\text{-} \rightarrow \beta'\text{-} \rightarrow \beta''\text{-}$ upon heating/cooling of $\sim 65 \text{ wt\%}$ of the sample. These results reveal that the type of gas (Ar or H_2) and partial pressures have little influence on the characteristic bond lengths observed in the five polymorphs, which contrasts the strongly influence on the stability of the different polymorphs and the sample composition.

Neodymium borohydride, $\text{Nd}(\text{BH}_4)_3$, is also synthesized and the polymorphic transitions are compared to $\text{Pr}(\text{BH}_4)_3$. The smaller voids in $\text{Nd}(\text{BH}_4)_3$ are not large enough to allow the rotation of $\text{Nd}(\text{BH}_4)_6$ octahedra and formation of a rhombohedral polymorphs. However, the stepwise polymorphic transitions $\beta\text{-} \rightarrow \beta'\text{-} \rightarrow \beta''\text{-}$ are also observed for this compound in the presence of hydrogen gas ($p(\text{H}_2) = 98 \text{ bar}$) and the sample completely transforms to $\beta''\text{-Nd}(\text{BH}_4)_3$ at $T = 269 \text{ }^\circ\text{C}$.

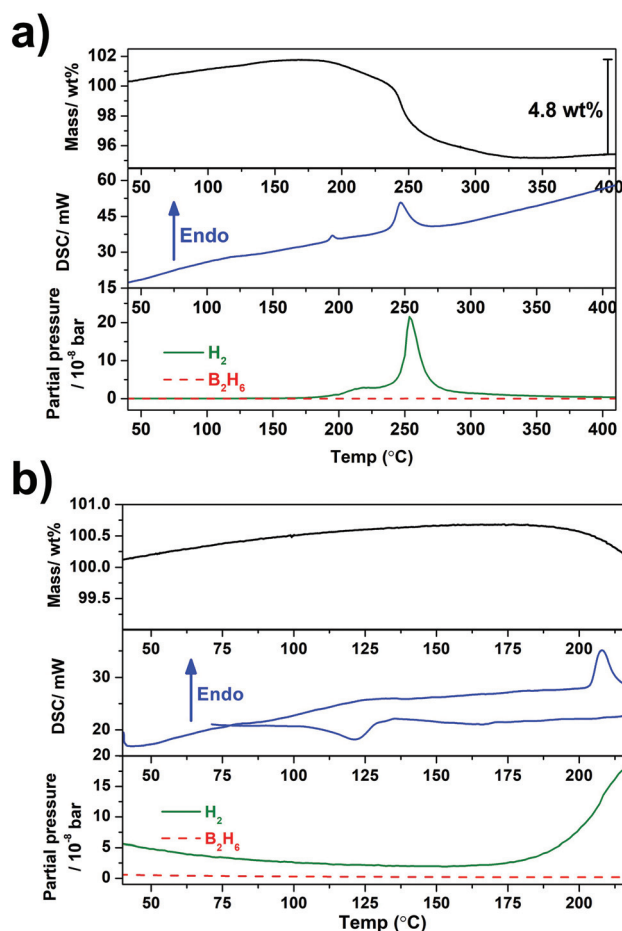


Fig. 9 (a) TGA-DSC-MS data for $\text{Pr}(\text{BH}_4)_3$ (s3) heated from RT to $400 \text{ }^\circ\text{C}$ (in argon flow). Upper part: The TGA curve in black. Middle: DSC curve in blue and the corresponding MS signals in the lower part for hydrogen and diborane presented by green and red curves, respectively. (b) TGA-DSC-MS data for $\text{Pr}(\text{BH}_4)_3$ (s3) heated from RT to $220 \text{ }^\circ\text{C}$ and cooled back to RT ($\Delta T/\Delta t = 5 \text{ }^\circ\text{C min}^{-1}$).

1 Here we present two very rare examples of stepwise negative
thermal expansion. More detailed structural analysis, *e.g.* also
including spectroscopy and advanced neutron scattering, may
5 provide further insight into both static and dynamic structural
effects. The *in situ* neutron powder diffraction experiment at
elevated temperature and pressures of different gasses is time
consuming but might be feasible with advanced neutron
sources.⁶¹ Further structural knowledge of the origin of step-
wise negative thermal expansion may allow rational design
10 and synthesis of novel types of technologically important nega-
tive or zero thermal expansion materials.

15 Conflicts of interest

Q6 ■■■■




20 Acknowledgements

The research leading to these results has received funding
from the People Program (Marie Curie Actions) of the
European Union's Seventh Framework Program FP7/
25 2007–2013/under REA grants agreement no. 607040 (Marie
Curie ITN ECOSTORE). Furthermore, this work was supported
by the Danish National Research Foundation, Center for
Materials Crystallography (DNRF93), the Danish Research
Council for Nature and Universe (Danscatt) and Danish
30 council for independent research (HyNanoBorN), DFF – 4181-
00462. NordForsk and The Nordic Neutron Science Program is
acknowledged for funding of FunHy (Project no. 81942). We
are grateful to the Carlsberg Foundation. The access to the
SNBL beamline at the ESRF Synchrotron, P02 beamline at
35 Petra (III) synchrotrons and SINQ at the Paul Scherrer institute
is gratefully acknowledged.

40 References

- 1 L. Schlapbach and A. Züttel, Hydrogen-storage materials
for mobile applications, *Nature*, 2001, **414**, 353–358.
- 2 R. Mohtadi and S. Orimo, The renaissance of hydrides as
45 energy materials, *Nat. Rev. Mater.*, 2016, **2**, 16091.
- 3 T. He, P. Pachfule, H. Wu, Q. Xu and P. Chen, Hydrogen
carriers, *Nat. Rev. Mater.*, 2016, **1**, 16059.
- 4 L. H. Jepsen, M. B. Ley, Y.-S. Lee, Y. W. Cho, M. Dornheim,
J. O. Jensen, Y. Filinchuk, J. E. Jørgensen, F. Besenbacher
50 and T. R. Jensen, Boron–nitrogen based hydrides and reac-
tive composites for hydrogen storage, *Mater. Today*, 2014,
17, 129–135.
- 5 M. B. Ley, L. H. Jepsen, Y.-S. Lee, Y. W. Cho, J. M. Bellosta
von Colbe, M. Dornheim, M. Rokni, J. O. Jensen, M. Sloth,
Y. Filinchuk, J. E. Jørgensen, F. Besenbacher and
T. R. Jensen, Complex hydrides for hydrogen storage – new
55 perspectives, *Mater. Today*, 2014, **17**, 122–128.

- 6 S. Orimo, Y. Nakamori, J. R. Eliseo, A. Zu and C. M. Jensen,
1 Complex Hydrides for Hydrogen Storage, *Chem. Rev.*, 2007,
107, 4111–4132.
- 7 M. Paskevicius, L. H. Jepsen, P. Schouwink, R. Černý,
D. B. Ravnsbæk, Y. Filinchuk, M. Dornheim,
5 F. Besenbacher and T. R. Jensen, Metal Borohydrides and
derivatives - synthesis, structure and properties, *Chem. Soc.
Rev.*, 2017, **46**, 1565–1634.
- 8 Y. Nakamori, K. Miwa, A. Ninomiya, H. Li, N. Ohba,
S. Towata, A. Züttel and S. Orimo, Correlation between
10 thermodynamical stabilities of metal borohydrides and
cation electronegativities: First-principles calculations and
experiments, *Phys. Rev. B: Condens. Matter Mater. Phys.*,
2006, **74**, 45126.
- 9 M. Heere, S. P. GharibDoust, M. Brighi, C. Frommen,
15 T. R. Jensen and B. C. Hauback, Hydrogen Sorption in
Erbium Borohydride Composite Mixtures with LiBH₄ and/
or LiH, *Inorganics*, 2017, **5**, 31.
- 10 M. Heere, S. P. GharibDoust, M. H. Sørby, C. Frommen,
T. R. Jensen and B. C. Hauback, In situ investigations of bi-
metallic potassium erbium borohydride, *Int. J. Hydrogen*
20 *Energy*, 2017, **42**, 22468–22474.
- 11 C. Frommen, M. Heere, M. D. Riktor, M. H. Sørby and
B. C. Hauback, Hydrogen storage properties of rare earth
25 (RE) borohydrides (RE=La, Er) in composite mixtures with
LiBH₄ and LiH, *J. Alloys Compd.*, 2015, **645**, S155–S159.
- 12 S. P. GharibDoust, D. B. Ravnsbæk, R. Černý and
T. R. Jensen, Synthesis, structure and properties of bi-
metallic sodium rare-earth (RE) borohydrides, NaRE(BH₄)₄,
30 RE = Ce, Pr, Er or Gd, *Dalton Trans.*, 2017, **46**, 13421–13431.
- 13 S. P. GharibDoust, M. Heere, M. H. Sørby, M. B. Ley,
D. B. Ravnsbæk, B. C. Hauback, R. Černý and T. R. Jensen,
Synthesis, structure and properties of new bimetallic
35 sodium and potassium lanthanum borohydrides, *Dalton
Trans.*, 2016, **45**, 19002–19011.
- 14 C. Frommen, M. H. Sørby, M. Heere, T. D. Humphries,
J. E. Olsen and B. C. Hauback, Rare Earth Borohydrides—
Crystal Structures and Thermal Properties, *Energies*, 2017,
40 **10**, 2115.
- 15 S. Marks, J. G. Heck, M. H. Habicht, P. On, C. Feldmann
and P. W. Roesky, [Ln(BH₄)₂(THF)₂] (Ln = Eu, Yb) Highly
Luminescent Material. Synthesis, Properties, Reactivity,
and NMR Studies, *J. Am. Chem. Soc.*, 2012, **2**, 16983–16986.
- 16 F. Bonnet, A. R. Cowley, P. Mountford, M. Road and O. Ox,
45 Lanthanide Borohydride Complexes Supported by
Diaminobis (phenoxide) Ligands for the Polymerization of
E-Caprolactone and L - and rac-Lactide, *Inorg. Chem.*, 2005,
44, 9046–9055.
- 17 F. Bonnet, M. Visseaux, A. Pereira and D. Barbier-Baudry,
Highly trans-stereospecific isoprene polymerization by neo-
dymium borohydrido catalysts, *Macromolecules*, 2005, **38**,
3162–3169.
- 18 S. M. Guillaume, M. Schappacher and A. Soum,
55 Polymerization of ε-Caprolactone initiated by Nd
(BH₄)₃(THF)₃: Synthesis of hydroxytelechelic poly(ε-capro-
lactone), *Macromolecules*, 2003, **36**, 54–60.

- 1  9 M. Heere, S. H. Payandeh, C. Frommen, T. D. Humphries, M. B. Ley, M. H. Sørby, T. R. Jensen and B. C. Hauback, The influence of LiH on the rehydrogenation behavior of halide free rare earth (RE) borohydrides (RE = Pr, Er), *Phys. Chem. Chem. Phys.*, 2016, **18**, 24387–24395.
- 5  10 D. B. Ravnsbæk, Y. Filinchuk, R. Černý, M. B. Ley, D. Haase, H. J. Jakobsen, J. Skibsted and T. R. Jensen, Thermal polymorphism and decomposition of $\text{Y}(\text{BH}_4)_3$, *Inorg. Chem.*, 2010, **49**, 3801–3809.
- 10 21 T. D. Humphries, M. B. Ley, C. Frommen, K. T. Munroe, T. R. Jensen and B. C. Hauback, Crystal structure and in situ decomposition of $\text{Eu}(\text{BH}_4)_2$ and $\text{Sm}(\text{BH}_4)_2$, *J. Mater. Chem. A*, 2015, **3**, 691–698.
- 15 22 K. Park, H.-S. Lee, A. Remhof, Y.-S. Lee, Y. Yan, M.-Y. Kim, S. J. Kim, A. Züttel and Y. W. Cho, Thermal properties of $\text{Y}(\text{BH}_4)_3$ synthesized via two different methods, *Int. J. Hydrogen Energy*, 2013, **38**, 9263–9270.
- 20 23 J. E. Olsen, C. Frommen, T. R. Jensen, M. D. Riktor, M. H. Sørby and B. C. Hauback, Structure and thermal properties of composites with RE-borohydrides (RE = La, Ce, Pr, Nd, Sm, Eu, Gd, Tb, Er, Yb or Lu) and LiBH_4 , *RSC Adv.*, 2014, **4**, 1570–1582.
- 25 24 M. Sharma, E. Didelot, A. Spyratou, L. M. Lawson Daku, R. Černý and H. Hagemann, Halide Free $\text{M}(\text{BH}_4)_2$ (M = Sr, Ba, and Eu) Synthesis, Structure, and Decomposition, *Inorg. Chem.*, 2016, **55**, 7090–7097.
- 30 25 M. Paskevicius, D. A. Sheppard, K. Williamson and C. E. Buckley, Metal hydride thermal heat storage prototype for concentrating solar thermal power, *Energy*, 2015, **88**, 469–477.
- 35 26 J. C. Crivello, R. V. Denys, M. Dornheim, M. Felderhoff, D. M. Grant, J. Huot, T. R. Jensen, P. de Jongh, M. Latroche, G. S. Walker, C. J. Webb and V. A. Yartys, Mg-based compounds for hydrogen and energy storage, *Appl. Phys. A: Mater. Sci. Process.*, 2016, **122**, 1–17.
- 40 27 M. B. Ley, D. B. Ravnsbæk, Y. Filinchuk, Y.-S. Lee, R. Janot, Y. W. Cho, J. Skibsted and T. R. Jensen, $\text{LiCe}(\text{BH}_4)_3\text{Cl}$, a New Lithium-Ion Conductor and Hydrogen Storage Material with Isolated Tetranuclear Anionic Clusters, *Chem. Mater.*, 2012, **24**, 1654–1663.
- 45 28 E. Roedern, Y.-S. Lee, M. B. Ley, K. Park, Y. W. Cho, J. Skibsted and T. R. Jensen, Solid state synthesis, structural characterization and ionic conductivity of bimetallic alkali-metal yttrium borohydrides $\text{MY}(\text{BH}_4)_4$ (M = Li and Na), *J. Mater. Chem. A*, 2016, **4**, 8793–8802.
- 50 29 Y.-S. Lee, M. B. Ley, T. R. Jensen and Y. W. Cho, Lithium Ion Disorder and Conduction Mechanism in $\text{LiCe}(\text{BH}_4)_3\text{Cl}$, *J. Phys. Chem. C*, 2016, **120**, 19035–19042.
- 55  30 M. B. Ley, S. Boulineau, Y. Filinchuk and T. R. Jensen, New Li Ion Conductors and Solid State Hydrogen Storage Materials: $\text{LiM}(\text{BH}_4)_3\text{Cl}$, M = La, Gd, *J. Phys. Chem. C*, 2012, **116**, 21267–21276.
- 1 S. P. GharibDoust, M. Brighi, Y. Sadikin, D. B. Ravnsbæk, R. Černý, T. R. Jensen and J. Skibsted, Synthesis, Structure and Li Ion Conductivity of $\text{LiLa}(\text{BH}_4)_3\text{X}$, X = Cl, Br, I, *J. Phys. Chem. C*, 2017, **121**, 19010–19021.
- 32 P. Schouwink, E. Didelot, Y.-S. Lee, T. Mazet and R. Černý, Structural and magnetocaloric properties of novel gadolinium borohydrides, *J. Alloys Compd.*, 2016, **664**, 378–384.
- 33 R. Černý and P. Schouwink, The crystal chemistry of inorganic metal borohydrides and their relation to metal oxides, *Struct. Sci. Cryst. Eng. Mater.*, 2015, **B71**, 619–640.
- 34 M. B. Ley, M. Jørgensen, R. Černý, Y. Filinchuk and T. R. Jensen, From $\text{M}(\text{BH}_4)_3$ (M = La, Ce) Borohydride Frameworks to Controllable Synthesis of Porous Hydrides and Ion Conductors, *Inorg. Chem.*, 2016, **55**, 9748–9756.
- 35 J. E. Olsen, C. Frommen, M. H. Sørby and B. C. Hauback, Crystal structures and properties of solvent-free $\text{LiYb}(\text{BH}_4)_{4-x}\text{Cl}_x$, $\text{Yb}(\text{BH}_4)_3$ and $\text{Yb}(\text{BH}_4)_{2-x}\text{Cl}_x$, *RSC Adv.*, 2013, **3**, 10764–10774.
- 36 M. B. Ley, M. Paskevicius, P. Schouwink, B. Richter, D. Sheppard, C. E. Buckley and T. R. Jensen, Novel solvates $\text{M}(\text{BH}_4)_3\text{S}(\text{CH}_3)_2$ and properties of halide-free $\text{M}(\text{BH}_4)_3$ (M = Y or Gd), *Dalton Trans.*, 2014, **43**, 13333–13342.
- 37 Y. Lee, J. Shim and Y. W. Cho, Polymorphism and Thermodynamics of $\text{Y}(\text{BH}_4)_3$ from First Principles, *J. Phys. Chem. C*, 2010, **114**, 12833–12837.
- 38 C. Frommen, N. Aliouane, S. Deledda, J. E. Fonnelløp, H. Grove, K. Lieutenant, I. Llamas-Jansa, S. Sartori, M. H. Sørby and B. C. Hauback, Crystal structure, polymorphism, and thermal properties of yttrium borohydride $\text{Y}(\text{BH}_4)_3$, *J. Alloys Compd.*, 2010, **496**, 710–716.
- 39 W. Wegner, T. Jaroń and W. Grochala, Preparation of a series of lanthanide borohydrides and their thermal decomposition to refractory lanthanide borides, *J. Alloys Compd.*, 2018, **744**, 57–63.
- 40 V. Dyadkin, P. Pattison, V. Dmitriev and D. Chernyshov, A new multipurpose diffractometer PILATUS@SNBL, *J. Synchrotron Radiat.*, 2016, **23**, 825–829.
- 41 B. R. S. Hansen, K. T. Møller, M. Paskevicius, A.-C. Dippel, P. Walter, C. J. Webb, C. Pistidda, N. Bergemann, M. Dornheim, T. Klassen, J.-E. Jørgensen and T. R. Jensen, In situ X-ray diffraction environments for high-pressure reactions, *J. Appl. Crystallogr.*, 2015, **48**, 1234–1241.
- 42 K. T. Møller, B. R. S. Hansen, A.-C. Dippel, J.-E. Jørgensen and T. R. Jensen, Characterization of Gas-Solid Reactions using In Situ Powder X-ray Diffraction, *Z. Anorg. Allg. Chem.*, 2014, **640**, 3029–3043.
- 43 P. Fischer, G. Frey, M. Koch, M. Konnecke, V. Pomjakushin, J. Schefer, R. Thut, N. Schlumpf, R. Burge, U. Greuter, S. Bondt and E. Berruyer, High-resolution powder diffractometer HRPT for thermal neutrons at SINQ, *Physica B: Condens. Matter*, 2000, **276–278**, 146–147.
- 44 B. C. Hauback, H. Fjellvåg, O. Steinsvoll, K. Johansson, O. T. Buset and J. Jørgensen, The high resolution Powder Neutron Diffractometer PUS at the JEEP II reactor at Kjeller in Norway, *J. Neutron Res.*, 2000, **8**, 215–232.
- 45 T. Roisnel and J. Rodriguez-Carvajal, *Computer program FULLPROF*, LLB-LCSIM, 2003.
- 46 P. Giannozzi, S. Baroni, N. Bonini, M. Calandra, R. Car, C. Cavazzoni, D. Ceresoli, G. L. Chiarotti, M. Cococcioni, I. Dabo, A. D. Corso, S. Fabris, G. Fratesi, S. de Gironcoli,

- 1 R. Gebauer, U. Gerstmann, C. Gougoussis, A. Kokalj, M. Lazzeri, L. Martin-Samos, N. Marzari, F. Mauri, R. Mazzarello, S. Paolini, A. Pasquarello, L. Paulatto, C. Sbraccia, S. Scandolo, G. Sclauzero, A. P. Seitsonen, A. Smogunov, P. Umari and R. M. Wentzcovitch, Quantum ESPRESSO: a modular and open-source software project for quantum simulations of materials, *J. Phys.: Condens. Matter*, 2009, **21**, 395502.
- 5 47 J. P. Perdew, K. Burke and M. Ernzerhof, Generalized gradient approximation made simple, *Phys. Rev. Lett.*, 1996, **77**, 3865–3868.
- 10 48 J. P. Perdew, Density-functional approximation for the correlation energy of the inhomogeneous electron gas, *Phys. Rev. B: Condens. Matter Mater. Phys.*, 1986, **33**, 8822–8824.
- 15 49 A. Otero-De-La-Roza and E. R. Johnson, Non-covalent interactions and thermochemistry using XDM-corrected hybrid and range-separated hybrid density functionals, *J. Chem. Phys.*, 2013, **138**, 204109.
- 20 50 A. Otero-de-la-Roza, E. R. Johnson and G. A. DiLabio, Halogen Bonding from Dispersion-Corrected Density-Functional Theory: The Role of Delocalization Error, *J. Chem. Theory Comput.*, 2014, **10**, 5436–5447.
- 25 51 A. Wolczyk, E. R. Pinatel, M. R. Chierotti, C. Nervi, R. Gobetto and M. Baricco, Solid-state NMR and thermodynamic investigations on $\text{LiBH}_4\text{-LiNH}_2$ system, *Int. J. Hydrogen Energy*, 2016, **41**, 14475–14483.
- 30 52 H. J. Monkhorst and J. D. Pack, Special points for Brillouin-zone integrations, *Phys. Rev. B: Solid State*, 1976, **13**, 5188–5192.
- 35 53 F. Franco, M. Baricco, M. R. Chierotti, R. Gobetto and C. Nervi, Coupling Solid-State NMR with GIPAW ab Initio Calculations in Metal Hydrides and Borohydrides, *J. Phys. Chem. C*, 2013, **117**, 9991–9998.
- 40 54 X. Zhang, Z. Wen, Z. Gu, X. Xu and Z. Lin, Synthesis and thermal behavior of the dawsonite-type solid solution $\text{K}_{1-x}(\text{NH}_4)_x\text{Al}(\text{OH})_2\text{CO}_3$, *Thermochim. Acta*, 2005, **433**, 116–120.
- 45 55 A. R. West, *Solid state chemistry and its application*, 2nd edn, 2014.
- 50 56 L. Hu, J. Chen, L. Fan, Y. Ren, Y. Rong, Z. Pan, J. Deng, R. Yu and X. Xing, Zero Thermal Expansion and Ferromagnetism in Cubic $\text{Sc}_{1-x}\text{M}_x\text{F}_3$ ($\text{M} = \text{Ga}, \text{Fe}$) over a Wide Temperature Range, *J. Am. Chem. Soc.*, 2014, **136**, 13566–13569.
- 55 57 L. Hu, J. Chen, A. Sanson, H. Wu, C. Guglieri Rodriguez, L. Olivi, Y. Ren, L. Fan, J. Deng and X. Xing, New Insights into the Negative Thermal Expansion: Direct Experimental Evidence for the ‘guitar-String’ Effect in Cubic ScF_3 , *J. Am. Chem. Soc.*, 2016, **138**, 8320–8323.
- 60 58 R. D. Shannon, Revised effective ionic radii and systematic studies of interatomic distances in halides and chalcogenides, *Acta Crystallogr., Sect. A: Cryst. Phys., Diffraction, Theor. Gen. Crystallogr.*, 1976, **32**, 751–767.
- 65 59 W. Wegner, T. Jaroń and W. Grochala, Polymorphism and hydrogen discharge from holmium borohydride, $\text{Ho}(\text{BH}_4)_3$, and $\text{KHo}(\text{BH}_4)_4$, *Int. J. Hydrogen Energy*, 2014, **39**, 20024–20030.
- 70 60 T. Sato, K. Miwa, Y. Nakamori, K. Ohoyama, H.-W. Li, T. Noritake, M. Aoki, S. Towata and S. Orimo, Experimental and computational studies on solvent-free rare-earth metal borohydrides $\text{R}(\text{BH}_4)_3$ ($\text{R} = \text{Y}, \text{Dy}, \text{and Gd}$), *Phys. Rev. B: Condens. Matter Mater. Phys.*, 2008, **77**, 104114.
- 75 61 M. Heere, M. J. Mühlbauer, A. Schökel, M. Knapp, H. Ehrenberg and A. Senyshyn, Energy research with neutrons (ErWiN) and installation of a fast neutron powder diffraction option at the MLZ, Germany¹, *J. Appl. Crystallogr.*, 2018, **51**, 1–5. 